NJC

Accepted Manuscript

This is an *Accepted Manuscript*, which has been through the Royal Society of Chemistry peer review process and has been accepted for publication.

Accepted Manuscripts are published online shortly after acceptance, before technical editing, formatting and proof reading. Using this free service, authors can make their results available to the community, in citable form, before we publish the edited article. We will replace this *Accepted Manuscript* with the edited and formatted *Advance Article* as soon as it is available.

You can find more information about *Accepted Manuscripts* in the Information for Authors.

Please note that technical editing may introduce minor changes to the text and/or graphics, which may alter content. The journal's standard Terms & Conditions and the Ethical guidelines still apply. In no event shall the Royal Society of Chemistry be held responsible for any errors or omissions in this *Accepted Manuscript* or any consequences arising from the use of any information it contains.

ROYAL SOCIETY OF CHEMISTRY

www.rsc.org/njc

Cite this: DOI: 10.1039/c0xx00000x

www.rsc.org/xxxxxx

ARTICLE TYPE

Synthesis of Hierarchically Porous ZSM-5 Zeolites by Steam-assisted Crystallization of Dry Gel Silanized with Short-chain Organosilane

Yicheng Zhang,[a] Kake Zhu,[a] Xinggui Zhou*[a] and Weikang Yuan[a]

Received (in XXX, XXX) Xth XXXXXXXXX 20XX, Accepted Xth XXXXXXXXX 20XX

DOI: 10.1039/b000000x

Three short-chain organosilanes, *i.e.,* 3-aminopropyltrimethoxy-silane (APTMS), [3-(2-aminoethyl)aminopropyl]trimethoxysilane (AEAPTMS) and phenylaminopropyltrimethoxysilane (PHAPTMS) were used for the synthesis of hierarchically micro-/mesoporous ZSM-5 zeolites by steam-assisted crystallization of silanized dry gels. Corresponding to the different moieties of organosilane, the obtained hierarchically porous ZSM-5 zeolites have different degrees of mesoporosity and exhibit spherical morphology composed of small nanounits. Among the three organosilanes, PHAPTMS with bulky cross-section is the most excellent mesopore directing agent. Tracking the structural evolution of PHAPTMS-ZSM-5 during crystallization shows that a large amount of mesopores are produced in the initial steaming, but it is confirmed not due to the presence of PHAPTMS. This initial mesoporosity is mostly preserved by the PHAPTMS molecules which inhibit the growth of crystalline phase and suppress the high mobility of aluminosilicate species under the steam atmosphere.

1 Introduction

Zeolites are extensively used in petrochemical industry as solid acid catalysts because of their inherent acidity and uniform micropore size (< 2 nm) that endow them with desirable shape-selectivity and thermal stability [1]. However, the sole presence of small-sized micropore network in zeolitic materials imposes big barrier for large molecules to diffuse in the pores and access the acid sites,[2,3] frequently leading to significant deterioration in catalytic performance[4,5]. Ordered mesoporous materials[6] with amorphous frameworks can facilitate the diffusion of large molecules, but they have weaker acidity and lower hydrothermal stability than microporous zeolites. Therefore, reducing the dimension of zeolite crystal downward to nanometer scale to lower the mass transfer resistance becomes a natural choice. However, the nanozeolites are difficult to handle and usually suffer from the problems of low yield in preparation and low thermal stability in application [7]. Alternatively, one can introduce mesopores into the zeolites to synthesize hierarchically porous zeolites (HPZs), which integrate the advantages of mesoporous materials and microporous materials.

Various approaches including hard templating,[8-11] soft templating,[12-15] dealumination[16,17] and desilication,[18,19] etc., have been established to synthesize zeolites with hierarchically pore structure. Silane-based method proposed by Serrano et al. in their review [20] is a very effective and widely adopted approach to derive HPZs. In principle, the condensable part of organosilane incorporates with the surface silanols of zeolitic frameworks by forming Si-O-Si bonds, and the organic part linked by a hydrothermal stable Si-C bond [21] inhibits the zeolite growth.

Different routes have been attempted to explore the most potential of organosilanes in generating mesoporosity in zeolites. The first successful fabrication of HPZs by organosilane was reported by Serrano et al. [22,23] They used short-chain organosilanes to silanize precrystallized zeolite seeds for inhibiting the further growth of zeolite crystal under high temperature hydrothermal treatment. Meanwhile, Pinnavaia et al.[24,25] used organosilanized polymer to generate small intracrystalline mesopores in MFI type zeolite. Afterwards, the silane-based methods were extrapolated by Li's group to synthesize HPZs (LTA, MFI) with intracrystalline mesopores by silanization of silica source.[26,27]

Hydrophobic long-alkyl-chain organosilanes always fail to modulate the growth of zeolite crystal in aqueous condition, because they are inevitably segregated from the aluminosilicate domain.[23,28] When long-chain organosilanes contain hydrophilic group in the chain[14,29] is used, they can play the role of mesoporogen in introducing mesopores into zeolites. However, the use of uncommon organosilanes restricts its wide application in industry.

All the above mentioned silane-based methods are within the scope of traditional hydrothermal synthesis. Recently, a silane-based dry gel method reported by Zhu et al. opens a new avenue to apply organosilane to the synthesis of HPZs.[30] After undergoing a solvent evaporation induced self-assembly (SEISA) process, dry gel with controlled morphology is formed with the participation of an inexpensive nonamphiphilic long-chain organosilane, *i.e.*, hexadecyltrimethoxysilane (HDTMS, Fig. 1). It is then subjected to steam treatment to generate mesoporous MFI zeolites.[30] This method does not entail the pre-crystallization step and makes the best use of water incompatible long-chain organosilane in synthesizing hierarchically porous

ZSM-5 zeolite. Moreover, because ethanol is used as a solvent to prepare the dry gel, uniform mixing of TEOS and organosilane is first achieved, and hydrolysis and condensation then occur upon the addition of TPAOH solution, yielding a dried aluminosilicate gel silanized with well-dispersed organosilane after evaporation of solvent.

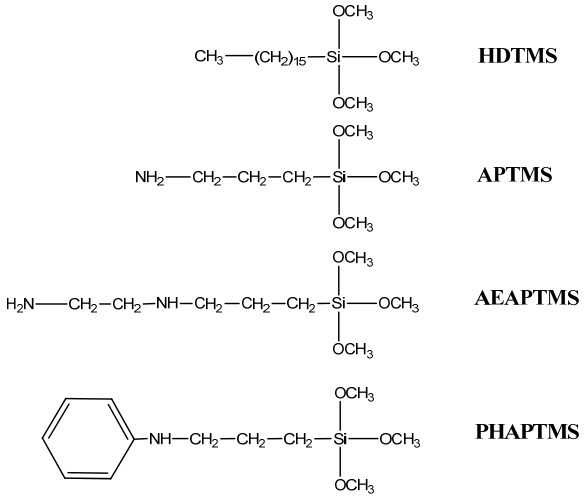

Fig. 1 Structure formulas of organosilanes including HDTMS, APTMS, AEAPTMS and PHAPTMS.

Up to now, either short- or long-chain organosilanes have been used for the synthesis of HPZs by silane-based method.[14, 23, 27-29] No reports are available in the literature successfully combining short-chain organosilane with dry gel method to generate hierarchically porous ZSM-5. Inspired by the successful short-chain organosilane assisted hydrothermal synthesis route to generate HPZs proposed by Serrano et al. [22,23], herein we explore the fabrication of hierarchically micro-/mesoporous ZSM-5 by steam-assisted crystallization of dry gel silanized with short-chain organosilane, which can also answer whether the long chain of the previously used HDTMS is a key factor in generating mesoscale pore structure by the silane-based dry gel method[30]. Three short-chain organosilanes, 3-aminopropyltrimethoxysilane (APTMS), [3-(2-aminoethyl)-aminopropyl]trimethoxysilane (AEAPTMS) and phenylamino-propyltrimethoxysilane (PHAPTMS), which have different organic moieties and are illustrated in Fig. 1, are used to pre-synthesize silanized dry gels. AEAPTMS and PHAPTMS additionally have an aminoethyl group and a phenyl group relative to APTMS, respectively. Compared with HDTMS, they all have a short chain length, though with different functional groups. With the three short-chain organosilanes, the silanized dry gels were subjected to steam treatment to synthesize hierarchically porous ZSM-5 zeolites, and the effect of their organic moiety size on mesopore generation in ZSM-5 zeolite was studied. Subsequently, the role of best-performing PHAPTMS in synthesizing hierarchically porous ZSM-5 zeolite was elucidated by tracking the structural evolution during steam treatment. Although this work is extended from the previous work [30], it has created its own style because the use of the short-chain organosilanes has produced HPZs with unique texture properties. It encourages us to stimulate the potential of other existing methods to synthesize new HPZ materials.

2 Experimental section

2.1 Synthesis of ZSM-5 zeolites

Three short-chain organosilanes (5% mol in regards to the TEOS addition amount) were selected for synthesis of hierarchically porous ZSM-5: APTMS, AEAPTMS and PHAPTMS. In a typical synthesis, ethanol solution A was prepared by dissolving 0.368 g PHAPTMS and 6 g tetraethyl orthosilicate (TEOS, 98%) in 23 g ethanol. Ethanol solution B was prepared by dissolution of 0.147 g aluminum isopropoxide (AIP) in 3.51 g tetrapropylammonium hydroxide (TPAOH, 25% wt) solution, followed by dilution with 30 g ethanol. Subsequently, the ethanol solution B was added to the ethanol solution A. The compositions of crude materials are followed: 0.025AIP: TEOS: 0.15TPAOH: 0.05PHAPTMS: $5H_2O$: 40EtOH. The clear solution was stirred at room temperature for 6 h to complete the hydrolysis of TEOS and followed by being dispersed in a dish for solvent evaporation under reduced pressure. It took 5-8 h to evaporate the solvent at room temperature in the drafty closet.

The as-prepared dry gel was transferred to a 10 ml Teflon cup, placed in a Teflon-lined autoclave (100 ml) with 10 g water at the bottom of the autoclave. The crystallization of the dry gel was carried out at 170 ^{o}C for 72 h. The products were washed, air-dried and finally calcined at 550 ^{o}C for 6 h to remove the structure-directing agent (SDA) and organosilane. The synthesized samples are denoted as O-ZSM-5, wherein O stands for the used organosilane (O = APTMS, AEAPTMS or PHAPTMS). For comparison, conventional ZSM-5 (denoted as ZSM-5) was synthesized under the similar procedures in the absence of organosilane.

Besides, the steam time of PHAPTMS-silanized dry gel was varied between 0 and 6 h to investigate the effect of crystallization time and the obtained materials after calcination are denoted as X-HPZ, where X is the length of time. The steam time of organosilane-free dry gel was varied between 0 and 3 h and the obtained materials after calcination are denoted as CON-Xh, where X is the length of time. The material after calcination of HDTMS-silanized dry gel is denoted as HDTMS-0h.

2.2 Characterization

X-ray diffraction (XRD) patterns were recorded with a Rigaku D/Max2550V diffractometer, with CuKα Radiation at 40 kV and 100 mA. The XRD patterns were collected in the range of 5−50° in $2\theta/\theta$ scanning mode with a 0.02° step and scanning speed of 12 degree/min. Nitrogen adsorption-desorption isotherms were measured on an ASAP 2010 (Micromeritics, USA) analyzer at -196 ^{o}C after the samples were degassed under vacuum for several hours at 250 ^{o}C. Specific surface area was calculated by the BET (Brunauer-Emmett-Teller) method based on the adsorption data at P/P_0 of 0.05-0.2. The external surface area and micropore volume were calculated using *t*-plots at P/P_0 of 0.1-0.4 (de Boer). The pore size distribution was calculated from the adsorption branch using the BJH (Barrett-Joyner-Halenda) method, and total pore volume was obtained from the adsorption at P/P_0 = 0.99. Scanning electron microscopy (SEM) images were recorded on a Hitachi 3400N Electron Microscope at an acceleration voltage of 15 kV. Transmission electron microscopy (TEM) images were obtained on a JEM-2100f instrument operated at 200 kV. All

samples subjected to TEM measurements were dispersed in ethanol ultrasonically and were dropped on copper grids. Solid state ^{27}Al MAS NMR spectra were recorded with an AVANCE 500 NMR spectrometer at a spinning frequency of 130.3 MHz. A 1.0 M solution of aluminum nitrate with a chemical shift 0.0 ppm was used as an external reference. Elemental analysis for the Si/Al ratio was performed with inductively coupled plasma optical emission spectroscopy (ICP-OES) using a SPECTRO ARCOS ICP Spectrometer.

3. Results and Discussion

3.1 Structure Characterization

Dry gels silanized with APTMS, AEAPTMS and PHAPTMS were subjected to steam treatment to respectively prepare APTMS-ZSM-5, AEAPTMS-ZSM-5 and PHAPTMS-ZSM-5, which are in comparison with ZSM-5 synthesized without organosilane. Fig. 2 shows the XRD patterns of conventional ZSM-5, APTMS-ZSM-5, AEAPTMS-ZSM-5 and PHAPTMS-ZSM-5. All diffraction patterns are found to be identical to the characteristics of the MFI topology,[31] demonstrating that the introduction of organosilanes does not stop the nucleation or growth of MFI zeolites. The absence of obvious amorphous diffraction pattern in the range between 20 to 30° suggests the almost complete conversion of the amorphous raw materials into crystalline zeolites. Compared with conventional ZSM-5, the materials synthesized with organosilane modifications have slightly lower intensity of XRD signals, indicating their smaller size of crystalline domains.

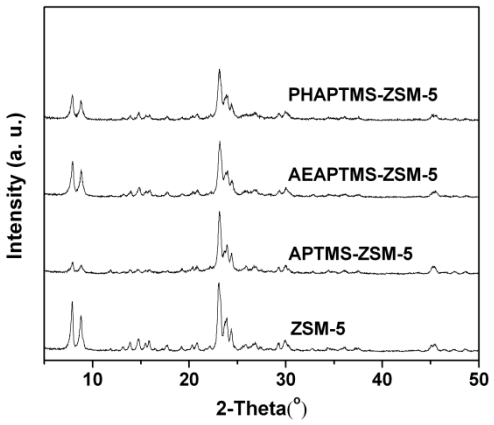

Fig. 2 XRD patterns of ZSM-5, APTMS-ZSM-5, AEAPTMS-ZSM-5 and PHAPTMS-ZSM-5.

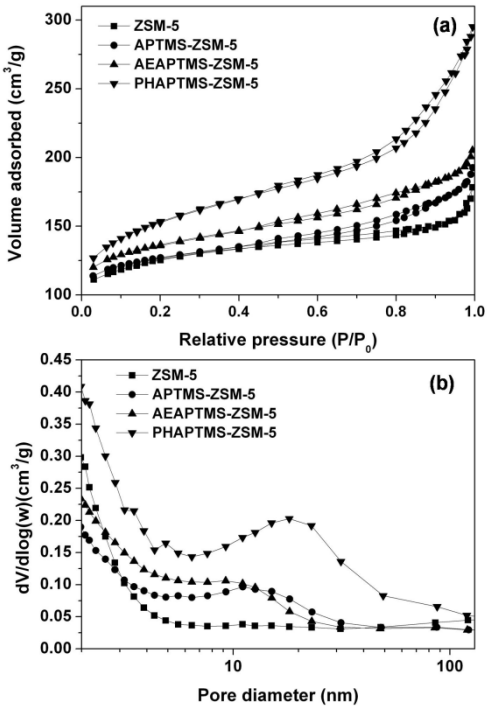

Fig. 3 ZSM-5 zeolites with different mesoporosity. (a) Nitrogen adsorption-desorption isotherms and (b) BJH pore size distributions derived from the adsorption branch.

Fig. 3 illustrates (a) the N_2 adsorption-desorption isotherms and (b) the corresponding Barrett-Joyner-Halenda (BJH) pore size distributions of these samples. All the isotherms exhibit the high adsorption amount of N_2 at relative low pressures (P/P_0 < 0.2), which are ascribed to the presence of inherent micropores in all samples. For conventional ZSM-5, a jump of N_2 uptake is observed only at a relative pressure close to 1 (Fig. 3a), probably attributed to the aggregation of small crystallites [25]. The isotherms of the three samples synthesized with organosilane modifications display a greater uptake of nitrogen at relative pressure of 0.2-0.95 (Fig. 3a), as resulted from the adsorption on the external surface and capillary effect insides mesopores. PHAPTMS-ZSM-5 exhibits a prominently steep slope in comparison with the rest samples, suggesting that it has the largest external surface area among all samples (Table 1). The adsorption-desorption isotherm of PHAPTMS-ZSM-5 belongs to a mixture of type I and IV with a type H3 hysteresis loop at relative pressure of 0.7-0.95 (Fig. 3a). The BJH pore size distribution (PSD) from the adsorption branch is in the range of 2-50 nm (Fig. 3b), and the additional broad peak between 6 and 50 nm compared with the PSD of conventional ZSM-5 is due to the effect of PHAPTMS. Comparatively, PSD calculated from desorption branch (Fig. S1) also has a similar distribution with the exception of the presence of the peak at 3.8 nm, which is attributed to the tensile strength effect (TSE)[32]. This peak can not represent the existence of mesopores in the material. Therefore, calculating PSD from adsorption branch is preferred in

Cite this: DOI: 10.1039/c0xx00000x

www.rsc.org/xxxxxx

ARTICLE TYPE

Table 1 Textural properties of ZSM-5 zeolites obtained by nitrogen physisorption experiments

Sample	Si/Al[a]	S_{BET}, [m^2/g]	S_{micro} [m^2/g] [b]	S_{ext} [m^2/g] [b]	V_{micro} [mL/g][b]	V_{meso} [mL/g] [c]
ZSM-5	40.5	429	303	126	0.14	0.14
APTMS-ZSM-5	43.2	430	298	132	0.13	0.17
AEAPTMS-ZSM-5	42.9	464	294	170	0.13	0.19
PHAPTMS-ZSM-5	43.4	530	262	268	0.12	0.34

[a] Determined by ICP-OES analysis; [b] Calculated from *t*-Plot method; [c] $V_{meso}=V_{ads,P/P0=0.99}-V_{micro}$.

this case. Compared with the highly mesoporous PHAPTMS-ZSM-5, the APTMS-ZSM-5 and AEAPTMS-ZSM-5, which also have higher degree of mesoporosity than conventional ZSM-5, appear to have not-so-typical characteristics of mesoporous materials. Despite this, they both possess newly formed mesopores around 5-30 nm. The texture data for the three materials are summarized in Table 1. Both the mesopore volume and external surface area of samples derived from silanized dry gel follows the order of APTMS-ZSM-5 < AEAPTMS-ZSM-5 < PHAPTMS-ZSM-5, revealing that the mesoporosity of zeolite increases with the moiety dimension of organosilane and PHAPTMS with bulky cross-section is the most effective mesopore directing agent for the synthesis of hierarchically micro-/mesoporous ZSM-5 zeolite. However, the organosilane size is much smaller than mesopore size, implying that the mesopores are not simply templated by organosilane.

The SEM images in Fig. 4a and TEM images in Fig. 5a and b show that the conventional ZSM-5 particles are irregularly shaped aggregates of loosely packed nanocrystals. The dot pattern of selected area electron diffraction (SAED) shown in Fig. 5b (inset) indicates that the nanocrystals are aligned in the same orientation. These conventional ZSM-5 particles are very similar to the HPZs obtained from the steam treatment of HDTMS-silanized dry gel (HDTMS-ZSM-5),[30] though with lower mesoporosity.

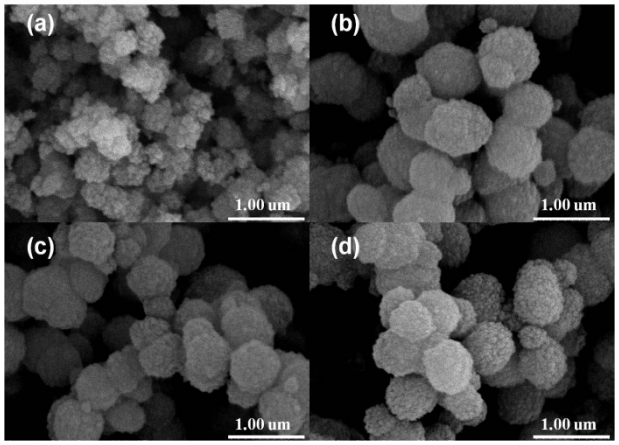

Fig. 4 SEM images of (a) ZSM-5, (b) APTMS-ZSM-5, (c) AEAPTMS-ZSM-5 and (d) PHAPTMS-ZSM-5.

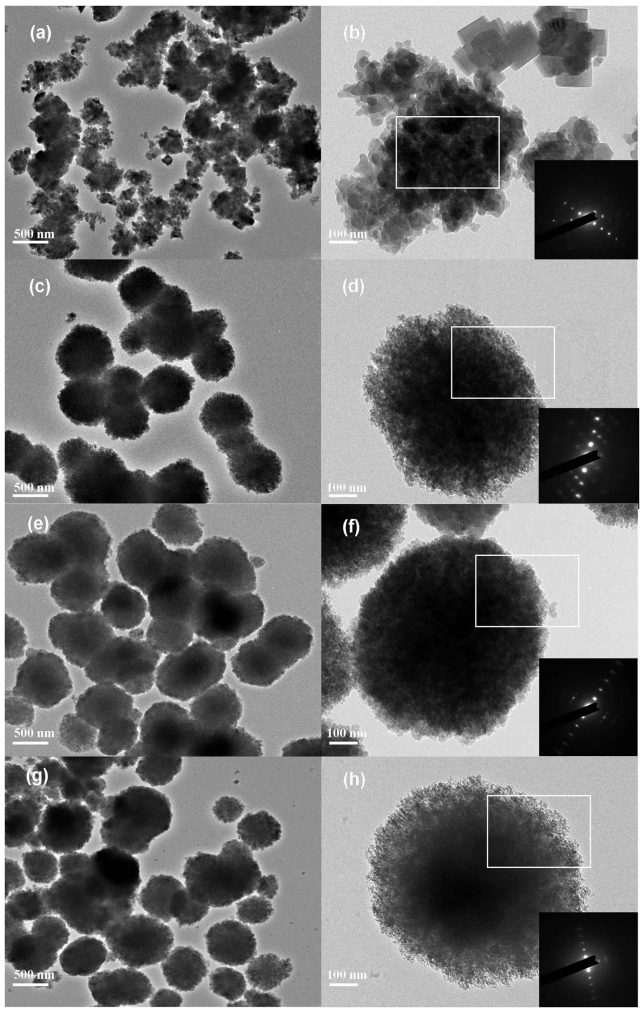

Fig. 5 TEM images of (a and b) ZSM-5, (c and d) APTMS-ZSM-5, (e and f) AEAPTMS-ZSM-5 and (g and h) PHAPTMS-ZSM-5. The insets in panels are the corresponding selected area electron diffraction patterns.

After the addition of short-chain organosilane, the morphology of the HPZs becomes significantly different from that of conventional ZSM-5. As shown in the SEM images (Fig. 4b-d), all three samples exhibit as spherical particles whose size varies in the range of 500-700 nm. Their sponge-like exterior surface

suggests that they are composed of small nanounits, which are not easily distinguishable through the insufficient SEM resolutions. The inhibiting effect of the organosilanes on crystal growth and the formation of spherical morphology can be confirmed irrespective of which short-chain organosilane is used. As shown in the TEM images (Fig. 5c-h), the mesoscale voids between the nanounits within the projected particle shapes are observed for the three samples. The dot patterns of SAED for the three samples (Fig. 5d, f and h, inset) not only show the crystalline nature of the nanounits within the zeolite particles, but also imply that the nanounits grow together with neighboring ones by the same orientation, similar to the case of orientated nanozeolite aggregates obtained by previous work [33].

The morphology of the hierarchically porous ZSM-5 zeolites is also related to the moiety dimension of short-chain organosilane. Among the three samples, the PHAPTMS-ZSM-5 particles have the fluffiest texture, once again reflecting the fact that PHAPTMS with bulky cross-section is most effective in the generation of mesopores in ZSM-5 zeolite. Although APTMS and AEAPTMS are effective in reducing the crystal size relative to conventional ZSM-5, APTMS-ZSM-5 and AEAPTMS-ZSM-5 contain fewer mesopores because of the smaller organic moiety of APTMS and AEAPTMS and the resulted closely contacted nanounits.

The three materials synthesized with short-chain organosilanes are different from HDTMS-ZSM-5 [30] in some respects. For simplicity, PHAPTMS-ZSM-5 as a representative is compared with HDTMS-ZSM-5. Both HDTMS and PHAPTMS serve as bond-blocking agents [27] and exert spatial separation effect on zeolite growth. However, HDTMS-ZSM-5 (0.49 mL/g) has a higher mesoporosity than PHAPTMS-ZSM-5 (0.34 mL/g), because the larger dimensional HDTMS occupies more space between the zeolitic walls. In other words, HDTMS with a carbon chain length of C16 has a stronger spatial separation effect than PHAPTMS with phenyl group of bulky cross-section. Besides, the different moiety dimensions of organosilanes also cause the morphological difference between the two samples. The large-sized long-chain HDTMS induces a relatively high degree of nanoscale segregation of organic-rich and organic-lean domains [28] (possibly due to self-assembly of HDTMS after evaporation of ethanol) in the dry gel, which is maintained during the zeolite growth. Therefore, the HDTMS-ZSM-5 units grow within a certain region of organic-lean domains (inorganic-rich domains where the inhibitor HDTMS cannot reach), and easily form rectangular shaped nanocrystals (10-50 nm), which are loosely packed into aggregates.[30] For PHAPTMS-ZSM-5, however, the dispersion of organic short-chain PHAPTMS in the inorganic materials is relatively homogeneous, and thus PHAPTMS can homogeneously inhibit the zeolite growth, resulting in smaller nanounits (5-10 nm, Fig. S2). However, PHAPTMS does not inhibit the nanounit by enclosing it, allowing the oriented assembly of nanounits into spherical aggregates of nanounits. Therefore, the size of crystalline domain increases, which has accounted for the the sharpening of diffraction peaks (Fig. 2). Having described the physical properties of the obtained materials, the synthesis route can be schematically illustrated in Fig. 6, where the clear solution containing hydrophilic moieties (AlO_{x-}, SiO_{x-} and TPAOH) silanized with short-chain organosilane is transformed into dry gel after solvent (ethanol) evaporation and the silanized dry gel is subjected to steam treatment to synthesize hierarchically porous ZSM-5.

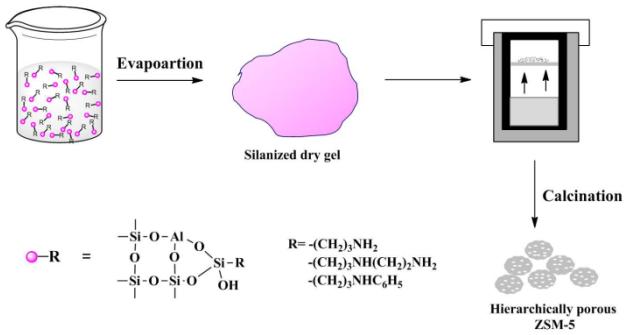

Fig. 6 Synthesis route of hierarchically porous ZSM-5 zeolites.

Besides, the state of the aluminium present in the hierarchically porous ZSM-5 is also the key to the performance of the material. Two representative samples, calcined ZSM-5 and PHAPTMS-ZSM-5, were selected for ^{27}Al MAS NMR measurement to reflect the aluminium coordination. In Fig. 7, the ^{27}Al MAS NMR spectra of both samples show an intense signal in at around 54 ppm and a weak signal centered at around 0 ppm, attributed to tetrahedrally coordinated framework aluminium and octahedral extraframework aluminium species, respectively [23]. This means that most Al atoms are incorporated into the framework and the silanization with organosilane does not influence the coordination state of Al atoms. The incorporation of aluminium into the framework has benefited from the accelerated dissolution and hydrolysis of aluminium isopropoxide by mixing it with TPAOH aqueous solution before adding ethanol during preparation of dry gel.

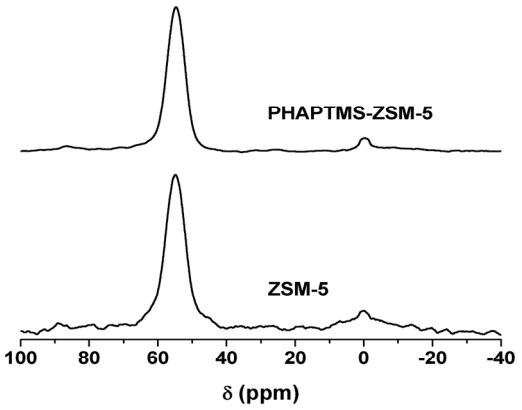

Fig. 7 ^{27}Al MAS NMR spectra of ZSM-5 and PHAPTMS-ZSM-5.

3.2 Structural Evolution of PHAPTMS-ZSM-5

We continue to focus our attention on the evolution of the crystallinity, porosity and morphology of the PHAPTMS-ZSM-5 material under steam treatment. The uncalcined dry gel particles have a size of several hundred micrometers and a smooth exterior surface (Fig. 8), which are very similar to the dry gel prepared with water as solvent [34] and are without any morphological relationship to the final submicron zeolite spheres. Therefore,

ethanol as solvent has no advantage in reducing the dry gel particle size, and the submicron zeolite spheres should have exclusively been formed during crystallization.

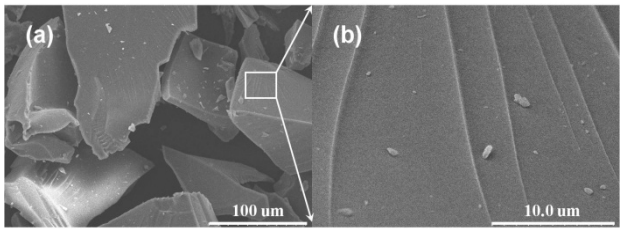

Fig. 8 SEM images of the uncalcined dry gel of (a and b) PHAPTMS-ZSM-5 prior to steam treatment.

The calcined dry gel of PHAPTMS-ZSM-5 (0-HPZ) is amorphous, as indicated by the XRD pattern shown in Fig. 9a. However, the amorphous phase, rather than crystalline ZSM-5, exhibits a type I (Langmuir) isotherm, typical for microporous materials (Fig. 9b). Similarly, the calcined dry gels of conventional ZSM-5 (CON-0h, Fig. S3) and HDTMS-ZSM-5 (HDTMS-0h, Fig. S4), which were prepared for comparison, also present the type I isotherm. As summarized in Table 2, the micropore volumes of 0-HPZ (0.21 mL/g), CON-0h (0.22 mL/g) and HDTMS-0h (0.24 mL/g) are comparable to each other. The abundant micropores in the calcined dry gel can be caused by the combustion of TPA^+ molecules inserted in the amorphous phase.[35] The calculated mesopore volume of the three calcined dry gels follows the order HDTMS-0h (0.14 mL/g) > 0-HPZ (0.05 mL/g) > CON-0h (0.02 mL/g), in line with our expectation that organosilane with larger organic moiety can generate more mesopores and calcined dry gel synthesized without organosilane has the fewest mesopores. Nevertheless, the small value of the mesopore volume of each sample and the slight difference among them suggest that both short-chain PHAPTMS and long-chain HDTMS do not develop well-defined mesopores in the dry gel prior to steaming. As shown in Fig. 10a and b, the calcined 0-HPZ still has the smooth and nonuniform morphology, which is almost the same as its uncalcined form (Fig. 8).

After steam treatment for 3 h, the obtained 3-HPZ exhibits a small peak at 22° on a large amorphous halo in the 2θ° angle range of 15-35° (Fig. 9a), which indicates the occurrence of crystal nucleation and initial crystal growth in the dry gel. Surprisingly, the isotherm appears in type IV with hysteresis loop (above P/P_0 = 0.7) that resembles type H1 (Fig. 9b) and the corresponding PSD curve shows a broad peak centered at 18 nm (Fig. 9b inset). As shown in Table 2, 3-HPZ has a relatively smaller micropore volume (0.17 mL/g) compared with 0-HPZ (0.21 mL/g), which suggests the smaller micropore volume of the emerging crystalline phase compared with that of the amorphous phase. However, it has a much higher mesopore volume (0.71 mL/g) and BET surface area (819 m^2/g), compared with those of 0-HPZ (0.05 mL/g and 582 m^2/g). Although 3-HPZ remains the shape of bulky dry gel (Fig. 10c), a high-magnification view of the bulky particle obviously reveals the surface roughness, which is caused by the appearance of small particles (Fig. 10d). Therefore, the bulky dry gel particle serves as a large amorphous matrix with embedded nanoparticles during crystallization.

After another 3 h of steaming, the obtained 6-HPZ has the XRD pattern with the typical peaks of MFI structure and without detectable amorphous background (Fig. 9a). The micropore volume decreases further, and the volume of initially formed abundant mesopores also decreases (Table 2). In addition, the N_2 adsorption-desorption isotherm has transformed into a mixture of type I and IV and the hysteresis loop has changed from type H1 to H3 (Fig. 9b). During the 3 hour steam treatment, the small particles crystallize further and tend to aggregate, leading to the more rugged surface of the matrix originated from dry gel (Fig. 10e), and the more visible particles with the size about several hundred nanometers in the matrix (Fig. 10e and f). Fig. 10g and h show the TEM images of some small 6-HPZ particles detached from the matrix by ultrasonic treatment. These particles are still in the form of loosely packed nanounits, which will assemble/grow with each other by the same orientation in the further steam treatment. In spite of the absence of amorphous background in XRD pattern, the presence of amorphous phase in the material cannot be excluded.

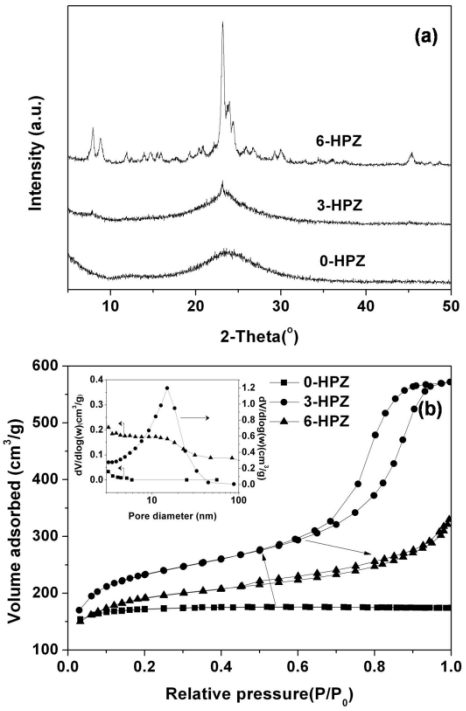

Fig. 9 (a) XRD patterns and (b) Nitrogen adsorption-desorption isotherms of 0-HPZ, 3-HPZ and 6-HPZ and inset BJH pore size distributions derived from the adsorption branch.

In contrast to the rapid and obvious changes during the first 6 h, further steaming the material until 72 h does not result in significant changes in the porosity of the material, as can be seen by comparing 6-HPZ with 72-HPZ (PHAPTMS-ZSM-5). Though the PHAPTMS molecules have not been efficient to avoid the rapid decrease of mesoporosity of the amorphous 3-HPZ, they have preserved the mesoporosity of the semi-crystalline 6-HPZ as far as possible. In this stage, the morphological changes are relatively obvious. Accompanied by the further amorphous-crystal transformation and the increase of crystallinity, the degree of intergrowth of small nanounits is enhanced, leading to the formation of well-developed zeolite submicron spheres (Fig. 4d, 5g and h). Besides, the dry gel matrix almost breaks up, as shown

in Fig. S5, which is an indication of the weak attachment between these zeolite spheres.

Table 2. Textural properties of PHAPTMS-ZSM-5 materials at various crystallization time and those of their counterparts.

Sample	S_{BET} [m^2/g]	S_{micro} [m^2/g] [a]	S_{meso} [m^2/g] [a]	V_{micro} [mL/g][a]	V_{meso} [mL/g][b]
0-HPZ	582	462	120	0.21	0.05
3-HPZ	819	381	438	0.17	0.71
6-HPZ	672	294	378	0.13	0.38
72-HPZ[c]	530	262	268	0.12	0.34
HDTMS-0h	808	538	270	0.24	0.14
CON-0h	583	479	104	0.22	0.02
CON-3h	557	283	274	0.13	0.59

[a] Calculated from *t*-Plot method; [b] $V_{meso}=V_{ads,P/P0\ =\ 0.99}-V_{micro}$; [c] namely PHAPTMS-ZSM-5, extracted from Table 1.

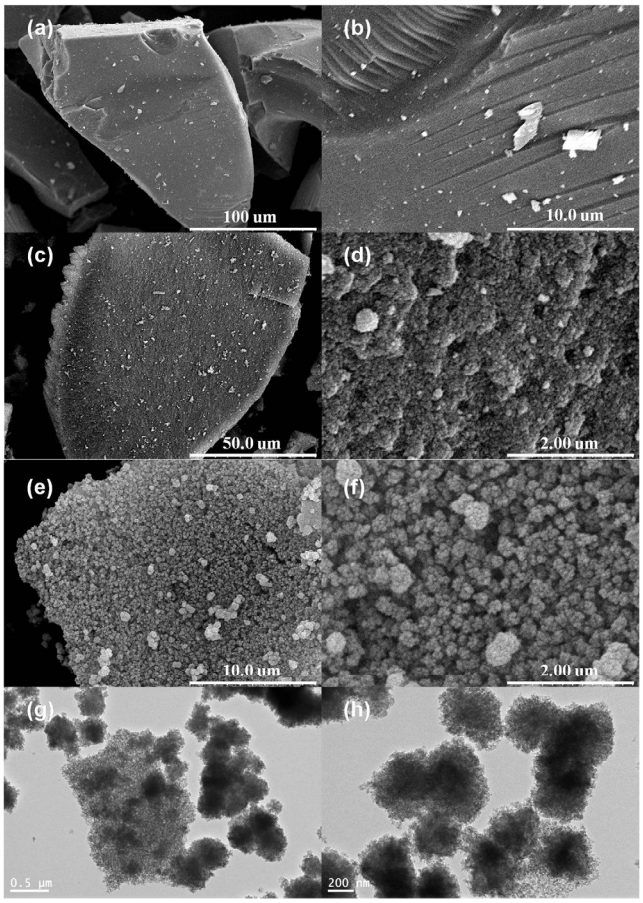

Fig. 10 SEM images of (a and b) 0-HPZ, (c and d) 3-HPZ, (e and f) 6-HPZ and (g and h) TEM images of 6-HPZ.

To determine whether the above phenomena are peculiar to the evolution of PHAPTMS-ZSM-5, we compare the results with those correspond to conventional ZSM-5 synthesized without organosilane. Prior to steam treatment, there are similarities between calcined CON-0h and 0-HPZ, as mentioned above. After steaming for 3 h, the CON-3h is semi-crystalline (Fig. S6), whereas the 3-HPZ is amorphous. 3-HPZ's lower conversion into crystalline phase within the same crystallization time once again proves the inhibiting effect of PHAPTMS on crystallization. It is interesting to see that CON-3h also has a substantial amount of mesopores with a PSD centered around 20 nm (Fig. S7 inset, Table 2), which is alike to 3-HPZ. The type H3 hysteresis loop in its isotherm (Fig. S7) may have been transformed from type H1, somewhat similar to the evolution of hysteresis loop from 3-HPZ to 6-HPZ. Comparing CON-3h with 3-HPZ, one can see that the initial formation of abundant mesopores does not rely on the presence of PHAPTMS.

However, the CON-3h contains a considerable amount of amorphous phase (observable amorphous background in Fig. S6 and residual amorphous phase in Fig. S8), indicating the low conversion of amorphous phase into crystalline zeolite. Although it possesses abundant mesopores, the existence of the amorphous phase makes the material less active and thermally unstable. By extending the time of steam treatment to 72 hours, the amorphous phase gradually disappears (Fig. 2). Meanwhile, the material experiences an inevitable dramatic decrease in mesoporosity (Fig. 3). Consequently, it eventually turns into the conventional ZSM-5 with poor mesoporosity.

During the nucleation and initial growth of PHAPTMS-ZSM-5 and conventional ZSM-5, the bulky gel disassembles into tiny particulates which are still arrested in the large dry gel matrix (Fig. 10c, d and S8). With next period of growth, the particulates gradually transform into nanocrystallites. For PHAPTMS-ZSM-5, the nanocrystallites or nanounits begin to undergo oriented assembly into aggregates with the inhibition of PHAPTMS (Fig. 10e, f and 5h). For conventional ZSM-5, however, the nanocrystallites tend to grow or fuse into relatively large nanocrystals due to the absence of PHAPTMS (Fig. 5b). After full crystallization, the aggregates of closely assembled nanounits (for PHAPTMS-ZSM-5) and aggregates of loosely packed nanocrystals (for conventional ZSM-5) substitute for their initial dry gel morphology, respectively.

PHAPTMS always plays a role of an inhibitor for crystallization via a Si–C bond-blocking principle. Despite this, the initially formed abundant mesopores are not imprinted by PHAPTMS and are generated during crystallization, regardless if PHAPTMS exists. When the material is subjected to steam treatment, the PHAPTMS molecules exert spatial separation effect, rather than serve as typical mesopore filling agents, to preserve the initial mesoporosity, indicating that high mobility of aluminosilicate sepcies is suppressed under the steam atmosphere with high humidity. Compared with Serrano's pioneering work [22,23], in which PHAPTMS silanizes pre-crystallized zeolite seeds to inhibit their growth and leads to narrow pore size distribution of the obtained zeolite materials, our silane-based dry gel method also employs a well-defined mechanism. In this method, PHAPTMS does not enclose and silanize a uniform core such as zeolite seed due to the absence of pre-crystallization step. The nucleation and the silanization take place simultaneously, and accordingly the growth of nucleation sites or nanounits is only partially inhibited by PHAPTMS, which permits the oriented intergrowth of generated nanounits and thus causes the rearrangement and relatively good preservation of initially formed mesopores. The materials are self-sustaining zeolite aggregates assembled from different-sized crystalline domains caused by different degrees of nanounits intergrowth and hence

they contain small- and large-sized mesopores, resulting in a broad pore size distribution. It is also noted that there are some important similarities between our silane-based dry gel method and Serrano's silane-based hydrothermal synthesis method [22,23]. In the two methods, the Si–C bond-blocking principle due to the condensable part of PHAPTMS and the spatial separation effect due to the bulky-cross section of PHAPTMS have a synergistic effect on influencing the zeolite growth. The preparation of silanized dry gel using ethanol as solvent before steam treatment and the silanization of zeolite seeds before elevated-temperature hydrothermal synthesis are necessary for the purpose of stimulating the most potential of PHAPTMS under their respective crystallization conditions.

Successful application of both long-chain [30] and short-chain organosilanes indicates that the mesoporosity and morphology of zeolite obtained by steaming-assisted crystallization of silanized dry gel depend on the dimension of organosilane, including the chain-length and/or the size of functional group.

4 Conclusions

The steam-assisted crystallization of dry gel silanized with short-chain organosilane was successful for the synthesis of hierarchically micro-/mesoporous ZSM-5. The mesoporosity of the obtained zeolites increases with the moiety dimension of short-chain organosilane. Among the three selected short-chain organosilanes, PHAPTMS with bulky cross-section is the best-performing mesopore directing agent which generates large mesopores (6-50 nm) in ZSM-5 and induces the formation of submicron zeolite spheres with the fluffiest texture. PHAPTMS always inhibits the growth of crystalline phase and mainly displays its role of mesoporogen in retaining the self-generated mesoporosity. This study suggests that the textural properties of hierarchically porous ZSM-5 obtained by this method can be tuned by varying organosilane type. This synthetic strategy is expected to be extended for more types of zeolites and considered to be a facile and general approach for synthesis of hierarchically porous zeolites.

Acknowledgments

X. G. Zhou is grateful for financial support from the National Basic Research Program of China (2012CB720501) and the Natural Science Foundation of China (U1162112). K. K. Zhu is sponsored by New Century Excellent Talents in University (NCET-11-0644) of the Chinese Department of Education.

Notes and references

[a] *State Key Laboratory of Chemical Engineering, East China University of Science and Technology, Shanghai, 200237, P. R. China. Fax: +86 21 64253528; Tel: +86 21 64253509; E-mail: xgzhou@ecust.edu.cn*

† Electronic Supplementary Information (ESI) available: [details of any supplementary information available should be included here]. See DOI: 10.1039/b000000x/

‡ Footnotes should appear here. These might include comments relevant to but not central to the matter under discussion, limited experimental and spectral data, and crystallographic data.

1. J. Čejka and S. Mintova, *Catal. Rev.*, 2007, **49**, 457.
2. K. Moller and T. Bein, *Chem. Soc. Rev.,* 2013, **42**, 3689.
3. M. S. Holm, E. Taarning, K. Egeblad and C. H. Christensen, *Catal. Today,* 2011, **168**, 3.
4. J. Kim, M. Choi and R. Ryoo, *J. Catal.,* 2010, **269**, 219.
5. V. N. Shetti, J. Kim, R. Srivastava, M. Choi and R. Ryoo, *J. Catal.,* 2008, **254**, 296.
6. D. Zhao, J. Sun, Q. Li and G. D. Stucky, *Chem. Mater.,* 2000, **12**, 275.
7. S. Mintova, J.-P. Gilson and V. Valtchev, *Nanoscale,* 2013, **5**, 6693.
8. C. J. H. Jacobsen, C. Madsen, J. Houzvicka, I. Schmidt and A. Carlsson, *J. Am. Chem. Soc.,* 2000, **122**, 7116.
9. W. Fan, M. A. Snyder, S. Kumar, P.-S. Lee, W. C. Yoo, A. V. McCormick, R. Lee Penn, A. Stein and M. Tsapatsis, *Nat Mater,* 2008, **7**, 984.
10. I. Schmidt, A. Boisen, E. Gustavsson, K. Ståhl, S. Pehrson, S. Dahl, A. Carlsson and C. J. H. Jacobsen, *Chem. Mater.,* 2001, **13**, 4416.
11. H. Zhu, Z. Liu, Y. Wang, D. Kong, X. Yuan and Z. Xie, *Chem. Mater.,* 2007, **20**, 1134.
12. F.-S. Xiao, L. Wang, C. Yin, K. Lin, Y. Di, J. Li, R. Xu, D. S. Su, R. Schlögl, T. Yokoi and T. Tatsumi, *Angew. Chem.,* 2006, **118**, 3162.
13. J. Yao, Y. Huang and H. Wang, *J. Mater. Chem.,* 2010, **20**, 9827.
14. M. Choi, H. S. Cho, R. Srivastava, C. Venkatesan, D.-H. Choi and R. Ryoo, *Nat. Mater.*, 2006, **5**, 718.
15. J. Jin, X. Zhang, Y. Li, H. Li, W. Wu, Y. Cui, Q. Chen, L. Li, J. Gu, W. Zhao and J. Shi, *Chem. Eur. J.* , 2012, **18**, 16549.
16. J. Lynch, F. Raatz and P. Dufresne, *Zeolites*, 1987, **7**, 333.
17. M. M. L. Ribeiro Carrott, P. A. Russo, C. Carvalhal, P. J. M. Carrott, J. P. Marques, J. M. Lopes, I. Gener, M. Guisnet and F. Ramôa Ribeiro, *Microporous Mesoporous Mater.,* 2005, **81**, 259.
18. D. Verboekend and J. Perez-Ramirez, *Catal. Sci. Technol.,* 2011, **1**, 879.
19. M. S. Holm, M. K. Hansen and C. H. Christensen, *Eur. J. Inorg. Chem.,* 2009, **2009**, 1194.
20. D. P. Serrano, J. M. Escola and P. Pizarro, *Chem. Soc. Rev.,* 2013, **42**, 4004.
21. K. Tsuji, C. W. Jones and M. E. Davis, *Microporous Mesoporous Mater.,* 1999, **29**, 339.
22. D. P. Serrano, J. Aguado, J. M. Escola, J. M. *Rodríguez* and Á. Peral, *Chem. Mater.,* 2006, **18**, 2462.
23. D. P. Serrano, J. Aguado, J. M. Escola, J. M. Rodriguez and A. Peral, *J. Mater. Chem.,* 2008, **18**, 4210.
24. H. Wang and T. J. Pinnavaia, *Angew. Chem. Int. Ed.,* 2006, **45**, 7603.
25. D. H. Park, S. S. Kim, H. Wang, T. J. Pinnavaia, M. C. Papapetrou, A. A. Lappas and K. S. Triantafyllidis, *Angew. Chem.,* 2009, **121**, 7781.
26. Z. Xue, J. Ma, W. Hao, X. Bai, Y. Kang, J. Liu and R. Li, *J. Mater. Chem.,* 2012, **22**, 2532.
27. Z. Xue, J. Ma, J. Zheng, T. Zhang, Y. Kang and R. Li, *Acta Mater.,* 2012, **60**, 5712.
28. R. Srivastava, N. Iwasa, S.-i. Fujita and M. Arai, *Chem. Eur. J.,* 2008, **14**, 9507.
29. R. R. Mukti, H. Hirahara, A. Sugawara, A. Shimojima and T. Okubo, *Langmuir,* 2009, **26**, 2731.
30. K. Zhu, J. Sun, J. Liu, L. Wang, H. Wan, J. Hu, Y. Wang, C. H. F. Peden and Z. Nie, *ACS Catalysis,* 2011, **1**, 682.
31. H. van Koningsveld, J. C. Jansen and H. van Bekkum, *Zeolites,* 1990, **10**, 235.
32. J. C. Groen, L. A. A. Peffer and J. Pérez-Ramírez, *Microporous Mesoporous Mater.,* 2003, **60**, 1.
33. D. P. Serrano, J. Aguado, J. M. Escola, A. Peral, G. Morales and E. Abella, *Catal. Today,* 2011, **168**, 86.
34. G. T. Neumann and J. C. Hicks, *Cryst. Growth. Des.,* 2013, **13**, 1535.
35. A. Corma, M. J. Diaz-Cabanas, M. Moliner and G. Rodriguez, *Chem. Commun.,* 2006, 3137.